Rheo-dielectrics in oligomeric and polymeric fluids: a review of recent findings

2003 J. Phys.: Condens. Matter 15 S909

(http://iopscience.iop.org/0953-8984/15/11/315)

INSTITUTE OF PHYSICS PUBLISHING JOURNAL OF PHYSICS: CONDENSED MATTER

J. Phys.: Condens. Matter **15** (2003) S909–S921 PII: S0953-8984(03)57916-4

Rheo-dielectrics in oligomeric and polymeric fluids: a review of recent findings

Hiroshi Watanabe[1], **Yumi Matsumiya and Tadashi Inoue**

Institute for Chemical Research, Kyoto University, Uji, Kyoto 611-0011, Japan

E-mail: hiroshi@scl.kyoto-u.ac.jp

Received 27 September 2002
Published 10 March 2003
Online at stacks.iop.org/JPhysCM/15/S909

Abstract

This paper gives a brief review of recent results of rheo-dielectric studies for oligo-styrene (OS) and *cis*-polyisoprene (PI). OS has type-B dipoles perpendicular to the backbone, and its dielectric α relaxation (glassy mode relaxation) is accelerated under the shear flow even at rates much smaller than the equilibrium relaxation frequency. This acceleration, resulting in the decrease of the viscosity (thinning) observed at those rates, is related to flow-induced reduction of the cooperativity of the segmental motion. For PI chains, having type-A dipoles parallel to the backbone, the dielectric relaxation detects the global chain motion. For well entangled PI chains, this relaxation is only moderately accelerated and its intensity is only mildly reduced even under fast flow in the non-Newtonian thinning regime. This result is related to a flow-induced orientational cross-correlation of entanglement segments. Within the context of the tube model for entangled chains, this cross-correlation can be related to the dynamic tube dilation induced by the convective constraint release.

1. Introduction

The central aim of rheological investigation is to specify a stress–strain relationship of a given material in both macroscopic and microscopic senses. In the microscopic (or molecular) sense, a stress-sustaining structure in the deformed material is specified and the motion of this structure resulting in the stress relaxation is examined. For example, for flexible polymer chains, an orientational anisotropy is the structural origin of the macroscopic stress and the thermal motion of the chains erasing this anisotropy results in the stress relaxation [1, 2].

Thus, the rheo-optical method combining structural and rheological measurements (such as the flow-birefringence measurement) has been widely utilized in rheological investigation of various materials [3, 4]. However, for this useful method to be applied, the material needs to be partially transparent to the utilized optical beam (e.g., light and x-rays). More importantly,

[1] Author to whom any correspondence should be addressed.

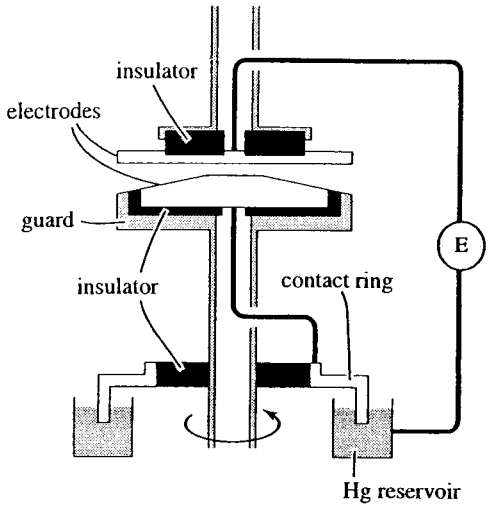

Figure 1. A schematic illustration of the cone-plate electrodes utilized in rheo-dielectric measurements.

the rheo-optical measurement usually detects just an *isochronal* average of the structure, and the molecular motion is observed as a time-dependent change of this average.

As a method complementary to this rheo-optical method, we recently focused on a rheo-dielectric method applicable to any materials having permanent electrical dipoles [5–10]. The rheo-dielectric signal intrinsically detects the motion of the dipoles (an orientational correlation at two *separate* times, say, 0 and t) and this motion can be converted to the motion of the molecules if the dipole arrangement with respect to the molecular axis is known. In fact, the rheo-dielectric measurements have revealed interesting features for the plastic flow mechanism of block copolymers [5], the shear orientation of liquid crystals [7–9] and the non-equilibrium relaxation in glassy and rubbery fluids, oligo-styrene (OS) and *cis*-polyisoprene (PI) [6, 10]. This article gives a brief review of the non-equilibrium behaviour of OS and PI thereby demonstrating the usefulness of the rheo-dielectric method.

2. Rheo-dielectric set-up

Figure 1 schematically shows the guarded, cone-plate-type electrodes for the rheo-dielectric measurement [5, 9, 10]. The sample was sandwiched between the cone and plate having a small gap angle (2°), and the cone head was flattened to avoid a direct contact of the electrodes. The electrodes were mounted on insulator blocks that were attached to a laboratory rheometer. The electrical contact to the steadily rotating electrode (cone electrode) was made through a contact ring dipped in a conducting liquid so that this rotation did not add noises on the rheo-dielectric signal. (A contact through a metal brush gave large noises and is not recommended.) Our measurements used mercury as the conducting liquid, but any liquid having a negligibly small electrical resistance can be utilized as a substitute.

For OS and PI samples under steady shear, a weak electric field was applied through the fixed and rotating (plate and cone) electrodes and the dielectric loss ε'' at the angular frequency ω was obtained. The ε'' at relatively high ω was measured under a sinusoidal electric field E, and the ε'' at low ω was obtained through Fourier transformation of an adsorption current under a rectangular field. Details of these modes of measurements were described elsewhere [6, 10].

The ε'' thus obtained under the shear at the rate $\dot{\gamma}$ is expressed in terms of the normalized dielectric relaxation function Φ and dielectric intensity $\Delta\varepsilon$ [11]

$$\varepsilon''(\omega;\dot{\gamma}) = -\Delta\varepsilon(\dot{\gamma})\int_0^\infty \frac{\mathrm{d}\Phi(t;\dot{\gamma})}{\mathrm{d}t}\sin\omega t\,\mathrm{d}t \qquad (\Phi(0;\dot{\gamma}) = 1). \tag{1}$$

In a stationary state under *local equilibrium*, these Φ and $\Delta\varepsilon$ can be related to a component of a microscopic polarization P_E in the direction of the electric field [11, 12],

$$\Phi(t;\dot{\gamma}) = \frac{\langle P_E(t)P_E(0)\rangle}{\langle P_E^2(0)\rangle}, \qquad \Delta\varepsilon(\dot{\gamma}) = K_\varepsilon'\langle P_E^2(0)\rangle \tag{2}$$

where K_ε' represents a constant determined by a ratio of the macroscopic and local electric field strengths and $\langle\cdots\rangle$ denotes an ensemble average. (In equation (2), an arbitrarily chosen reference time in the stationary state is set to be zero.)

The P_E, given as a sum of the dipoles, fluctuates with the time t according to the molecular motion and the dipole arrangement with respect to the molecular axis, and the molecular motion is affected by the shear flow. Thus, for the molecules of a known dipole arrangement, the shear effect on the molecular motion/conformation can be examined through the rheo-dielectric ε'' data.

3. Rheo-dielectric behaviour of OS and non-entangled PI [6]

3.1. Linear viscoelastic behaviour

Linear viscoelastic, storage and loss moduli G' and G'' were measured for OS ($M_w = 0.95\times10^3$, $M_w/M_n = 1.13$) and linear PI ($M_w = 8.2\times10^3$, $M_w/M_n = 1.05$) at temperatures T well above the glass transition point T_g, $T = 42\,^\circ$C (=T_g+35) for OS and $T = 23\,^\circ$C (=T_g+98) for PI. The results are summarized in figure 2. The viscoelastic relaxation seen here is induced by the equilibrium molecular motion that is negligibly affected by the applied, small strain (in the linear viscoelastic regime).

The molecular weight of OS is close to that of the Rouse segment ($M_s^{(R)} = 900$ for styrene [13]) and the OS molecules exhibit no significant internal flexibility. Correspondingly, the terminal relaxation of OS seen in figure 1(a) is assigned as the α relaxation due to the glassy mode (that is often referred to as the segmental mode) [14]. In relation to this point, we should note that the G' plateau before the relaxation has a height $\simeq 10^9$ Pa typical of glassy materials.

In contrast, the PI chain exhibits flexibility, and its terminal viscoelastic relaxation (figure 2(b)) occurs through the rubbery mode corresponding to the global chain motion [14]. At the same time, the PI chain is not sufficiently long to be entangled ($M_w < M_c = 10\times10^3$ with M_c being the characteristic molecular weight for entanglement [15]).

From the G' and G'' data shown in figure 2, the terminal viscoelastic relaxation time $\tau_{ve}(=[G'/\omega G'']_{\omega\to0})$ is evaluated to be [6]

$\tau_{ve} = 1.3\times10^{-5}$ s for the equilibrium segmental mode of OS at 42 °C (3)

$\tau_{ve} = 4.0\times10^{-5}$ s for the equilibrium global mode of PI at 23 °C. (4)

These τ_{ve} values provide us with a clue to discuss the steady flow and rheo-dielectric behaviour of OS and PI described below.

3.2. Steady flow and rheo-dielectric behaviour

Figure 3 shows the shear rate ($\dot{\gamma}$) dependence of the steady state viscosity $\eta(\dot{\gamma})$ measured for OS at 42 °C and PI at 23 °C (filled and unfilled circles). The dotted lines indicate plots of the

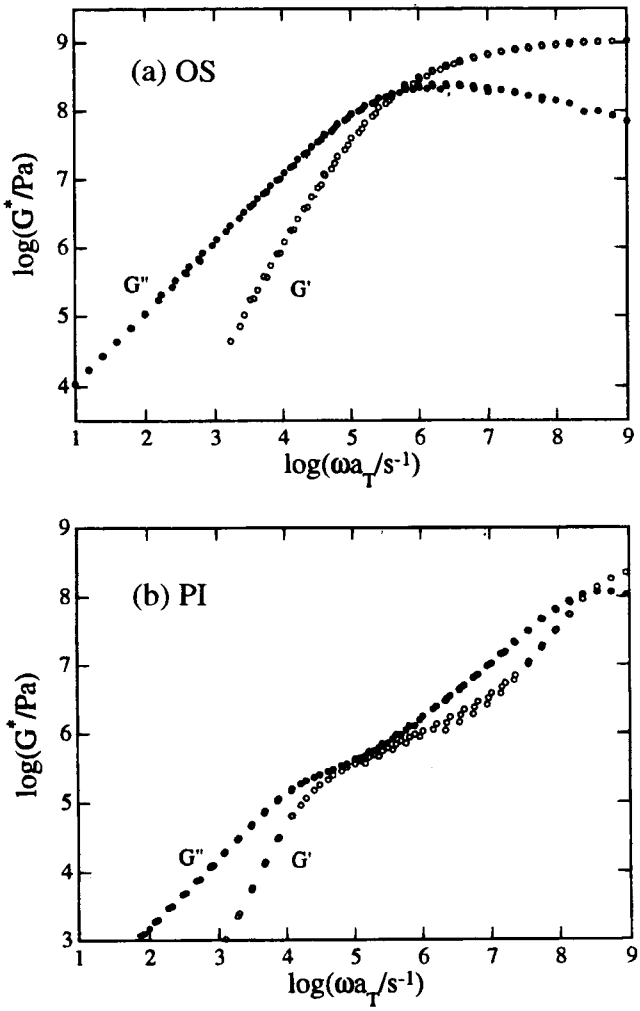

Figure 2. Linear viscoelastic moduli G' and G'' of (a) OS ($M_w = 0.95 \times 10^3$) at 42 °C and (b) non-entangled PI ($M_w = 8.2 \times 10^3$) at 23 °C. Redrawn, with permission, from 1998 *Macromolecules* **31** 7973–5. Copyright 1998 Am. Chem. Soc.

magnitude of complex viscosity $|\eta * (\omega)|$ against ω. The shear rates examined ($\leqslant 100\ s^{-1}$) are much smaller than the equilibrium relaxation frequency τ_{ve}^{-1} (cf equations (3) and (4)). The equilibrium global motion of the PI chains is not affected by such slow flow and thus the Newtonian behaviour ($\dot{\gamma}$-independent η that coincides with the zero-shear viscosity) is observed; cf unfilled circles. In contrast, the $\eta(\dot{\gamma})$ of OS significantly decreases (below $|\eta * (\omega)|_{\omega=\dot{\gamma}}$) with increasing $\dot{\gamma}$ up to 63 $s^{-1} \cong 8.2 \times 10^{-4}\tau_{ve}^{-1}$; cf filled circles. This extraordinarily strong thinning has also been observed for a glassy mode contribution to the elongational viscosity of a high-M polystyrene [14].

The origin of this thinning behaviour was examined though the rheo-dielectric test. The test was conducted for OS as well as for PI (for comparison) at the shear rates indicated with the arrows in figure 3. The results are summarized in figure 4. For both OS and PI, the terminal dielectric relaxation characterized by the proportionality between ε'' and ω is observed in our experimental window.

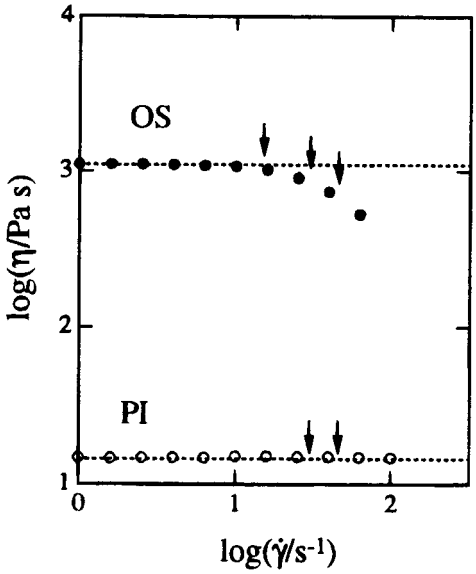

Figure 3. Steady state viscosity $\eta(\dot{\gamma})$ of OS ($M_w = 0.95 \times 10^3$) at 42 °C and non-entangled PI ($M_w = 8.2 \times 10^3$) at 23 °C. Plots of $|\eta*(\omega)|$ against ω are also shown (dotted lines). The arrows indicate the shear rates for the rheo-dielectric data shown in figure 4. Redrawn, with permission, from 1998 *Macromolecules* **31** 7973–5. Copyright 1998 Am. Chem. Soc.

The linear PI chain has the type-A dipoles [16] parallel along the chain backbone in addition to the type-B dipoles perpendicular to the backbone, and the polarization $P_E(t)$ fluctuating at long times is dominantly contributed from the type-A dipoles [17]: this P_E is proportional to the end-to-end vector of the chain [17, 18]. Thus, the terminal dielectric relaxation detecting the fluctuation of $P_E(t)$ (cf equations (1) and (2)) reflects the global chain motion (end-to-end vector fluctuation). As seen in figure 4(b), the ε'' data do not change with the slow shear at $\dot{\gamma} \leqslant 46\ \mathrm{s}^{-1}(\widetilde{=}1.8 \times 10^{-3}\tau_{ve}^{-1})$, demonstrating that the global chain motion at equilibrium is not affected by such slow shear. This result is in harmony with the Newtonian behaviour seen at those $\dot{\gamma}$ (cf figure 3(b)).

The OS molecule has only type-B dipoles and its terminal dielectric relaxation reflects the motion of monomeric segments (for the glassy mode [13, 14]). This relaxation is accelerated on the increase of $\dot{\gamma}$ up to $46\ \mathrm{s}^{-1}(\widetilde{=}6.0 \times 10^{-4}\tau_{ve}^{-1})$, as noted from the shift of the terminal tail ($\varepsilon'' \propto \omega$) toward the high-$\omega$ side; cf figure 4(a). Interestingly, the magnitude of this acceleration (by a factor $\widetilde{=}2$ for $\dot{\gamma} = 46\ \mathrm{s}^{-1}$) is similar to the magnitude of the decrease of η seen in figure 3(a). Thus, the strong thinning of OS is attributable to the acceleration of the segmental motion under slow shear at $\dot{\gamma} \ll \tau_{ve}^{-1}$. Although a quantitative analysis of this dielectrically detected acceleration of the segmental motion requires an evaluation of a magnitude of motional correlation of the type-B dipoles that may change with $\dot{\gamma}$ [18], the acceleration itself is sufficient for our qualitative discussion of the thinning mechanism presented below.

3.3. Thinning mechanism of OS

For homogeneous liquids, the thinning is usually observed *only* under fast flow at $\dot{\gamma} > \tau_{ve}^{-1}$ [19]. Nevertheless, the segmental motion of OS is accelerated to induce the thinning under slow flow at $\dot{\gamma} \sim \mathrm{O}(10^{-3}\tau_{ve}^{-1})$. This result suggests that the OS system includes some sort of

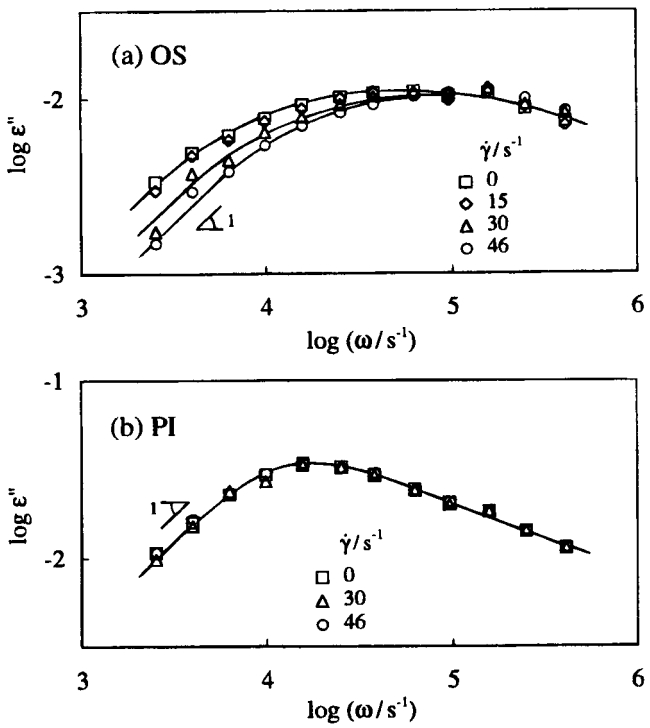

Figure 4. Dielectric loss ε'' of OS ($M_w = 0.95 \times 10^3$) at 42 °C and non-entangled PI ($M_w = 8.2 \times 10^3$) at 23 °C under steady shear flow. For comparison, the data at equilibrium ($\dot{\gamma} = 0$) are also shown. Redrawn, with permission, from 1998 *Macromolecules* **31** 7973–5. Copyright 1998 Am. Chem. Soc.

dynamically heterogeneous structure: such a structure can be distorted under the slow flow to affect the segmental motion therein and induce the thinning. A molecular dynamics simulation has revealed a related thinning feature for cluster-forming, supercooled liquids [20].

This dynamically heterogeneous structure in the OS system would be the cooperative domain structure [21] (and/or the conformer domain structure [22]) characteristic of glassy materials. In the timescale of segmental motion, this dynamic domain structure could have survived in the OS system even at $T = 43\,^{\circ}\mathrm{C} = T_g + 35$. Since the motion of the dynamic domain itself would be much slower than the motion of individual segments having the characteristic time τ_{ve}, the flow at $\dot{\gamma} \sim \mathrm{O}(10^{-3}\tau_{ve}^{-1})$ could be still faster than the domain motion to reduce the domain size/magnitude of cooperativity and accelerate the segmental motion.

3.4. Comment for the rheo-dielectric behaviour of PI

Here, a comment needs to be added for the rheo-dielectric behaviour of PI. For PI, the terminal relaxation occurring at τ_{ve} (equation (4)) reflects the global chain motion. The motion of the monomeric segments inducing the high-ω relaxation seen in figure 2(b) has a much shorter characteristic time, $\tau_s \cong 4 \times 10^{-9}$ s at 23 °C. Thus, the shear flow examined ($\dot{\gamma} \leqslant 10^2\ \mathrm{s}^{-1}$; cf figures 3 and 4) is *orders of magnitude* slower than the segmental motion ($\dot{\gamma}\tau_s \leqslant 4 \times 10^{-7}$). Under this slow flow, the dynamic heterogeneity is quite possibly smeared in the terminal regime to give no thinning/rheo-dielectric change.

Concerning this point, we remember that entangled chains exhibit significant thinning under flow slower than the segmental motion but faster than the global motion ($\dot{\gamma}\tau_{ve} > 1$) [1, 2]. Thus, rheo-dielectric changes may be observed for the entangled chains in the thinning regime. On the basis of this consideration, we examined those changes for highly entangled PI chains. The results are presented below.

4. Rheo-dielectric behaviour of entangled PI [10]

4.1. Overview

Steady flow and rheo-dielectric behaviour was examined for linear PI ($M_w = 1190 \times 10^3$, $M_w/M_n = 1.11$) and six-arm star PI (arm molecular weight $M_{arm} = 179 \times 10^3$, $M_w/M_n = 1.03$) dissolved in a low-M, vinyl-rich polybutadiene (B2; $M_w = 2 \times 10^3$, $M_w/M_n \cong 2$) at the PI concentrations $C_{PI} = 10$–25 wt% [10]. The PI chains were heavily entangled among themselves, and the number of entanglement segments per chain was $N_{chain} = 24$ and 36 for the linear PI at $C_{PI} = 10$ and 15 wt%, respectively, and $N_{chain} = 42$ and 54 for the star PI chain at $C_{PI} = 20$ and 25 wt%. (The B2 chains, the solvent, were too short to be entangled with the PI chains.)

Figure 5 shows the steady state viscosity η and the first normal stress coefficient Ψ_1 of the linear and star PI chains having $C_{PI} = 15$ and 20 wt%, respectively. The arrows indicate the terminal relaxation frequency in the linear viscoelastic regime, τ_{ve}^{-1}. This τ_{ve}^{-1} is equivalent to the frequency of the global motion of respective chains at equilibrium. Both η and Ψ_1 strongly decrease from respective zero-shear values (horizontal thick curves) with increasing $\dot{\gamma}$ above τ_{ve}^{-1}.

This type of thinning is characteristic of entangled chains and related to the strong orientation and non-equilibrium motion of the chains under flow [1, 2, 15]. For description of the orientation/motion in large spatial scales, the chain is conveniently coarse grained as a sequence of entanglement segments (of the molecular weight $M_e = CRT/G_N$ with R = gas constant, T = absolute temperature, and G_N = entanglement plateau modulus). The $\dot{\gamma}$ values examined here were larger than τ_{ve}^{-1} but smaller than the Rouse relaxation frequency τ_R^{-1} for the contour length fluctuation of the chain [10]. Thus, the entanglement segment can be safely regarded to have its equilibrium size a at those $\dot{\gamma}$.

The rheo-dielectric test was conducted at representative shear rates (for which the η and Ψ_1 data are shown with the filled symbols in figure 5). The ε'' data thus obtained are summarized in figure 6.

For the star PI (figure 6(b)), two broad ε''-peaks are observed at equilibrium ($\dot{\gamma} = 0$): the high-ω and low-ω peaks, respectively, correspond to the Rouse fluctuation of the arm contour length and the global chain motion having a larger motional amplitude compared to the Rouse fluctuation [10, 23]. Under the shear examined, the low-ω peak decreases its height and shifts to the higher-ω side. These rheo-dielectric changes indicate that the dielectric intensity $\Delta\varepsilon$ and the terminal dielectric relaxation time τ_ε decrease under the flow at $\dot{\gamma} > \tau_{ve}^{-1}$. In contrast, the dielectric behaviour of the linear PI chain is much less sensitive to the flow (figure 6(a)).

As a summary of these rheo-dielectric changes, figure 7 shows the $\Delta\varepsilon$ and τ_ε of the linear/star PI chains plotted against a normalized shear rate $\dot{\gamma}\tau_{ve}$. The thick horizontal lines indicate the equilibrium values of $\Delta\varepsilon$ and τ_ε. The flow-induced decreases of $\Delta\varepsilon$ and τ_ε are much smaller than the decreases of the viscoelastic η and Ψ_1 even for the star PI chains; cf figures 5 and 7. Similar results were found at all C_{PI} examined [10]. The origin of this difference between the dielectric and viscoelastic properties is discussed below.

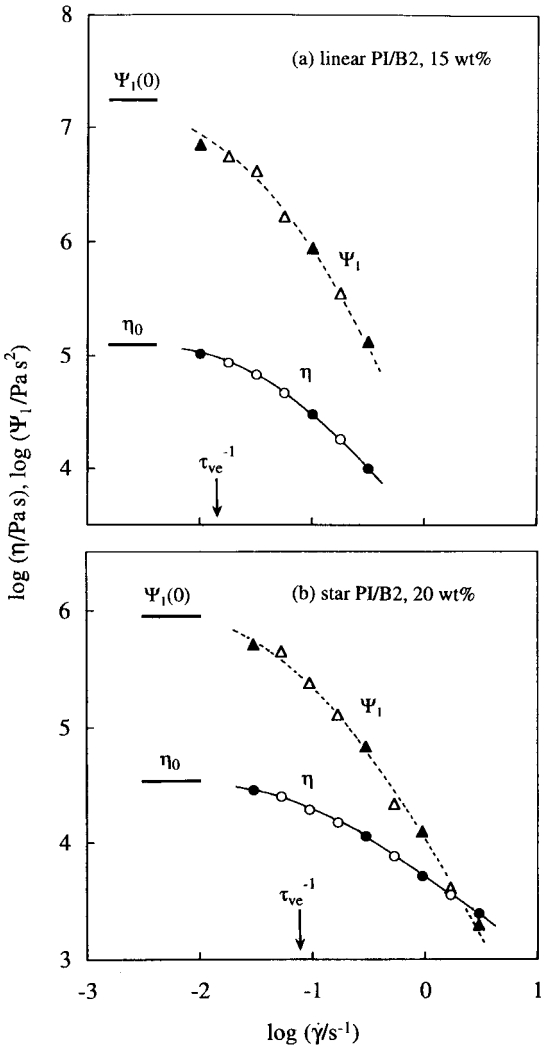

Figure 5. Steady state viscosity $\eta(\dot{\gamma})$ and first normal stress coefficient $\Psi_1(\dot{\gamma})$ of entangled linear PI ($M_w = 1190 \times 10^3$, $C_{PI} = 15$ wt%) at 30 °C and six-arm star PI ($M_{arm} = 179 \times 10^3$, $C_{PI} = 20$ wt%) at 25 °C. Redrawn, with permission, from 2002 *Macromolecules* **35** 8802–18. Copyright 2002 Am. Chem. Soc.

4.2. Orientational cross-correlation under shear flow

Here, we focus on the dielectric intensity $\Delta\varepsilon$ that detects the fluctuation amplitude of the microscopic polarization P_E in the direction of the electric field (chosen as the y direction); see equation (2). For the type-A linear and star chains unstretched under the shear flow at $\dot{\gamma} < \tau_R^{-1}$, the nth entanglement segment at the reference time 0 has the bond vector $\boldsymbol{u}(n, 0) = a\tilde{\boldsymbol{u}}(n, 0)$, where a and $\tilde{\boldsymbol{u}}(n, 0)$ are the equilibrium size and unit bond vector of the segment. A contribution of this segment to $P_E(0)$ is given by $\mu_o a\tilde{\boldsymbol{u}}(n, 0)$ with μ_o being the magnitude of the type-A dipole normalized to unit length of the chain contour. Thus, from equation (2), $\Delta\varepsilon$ is expressed

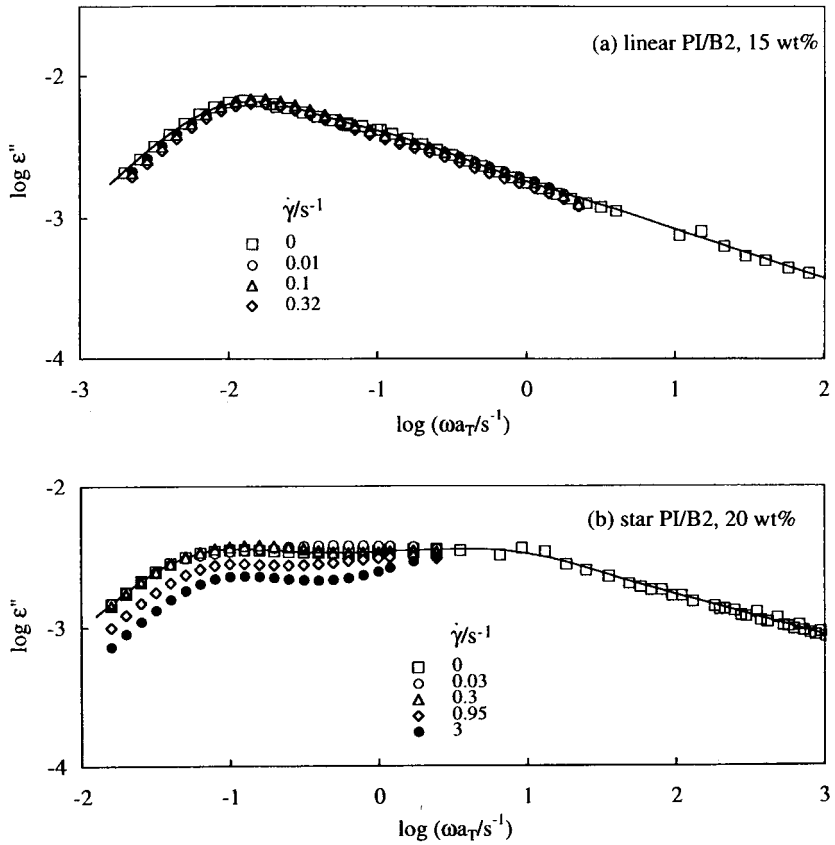

Figure 6. Rheo-dielectric behaviour of entangled linear PI ($M_w = 1190 \times 10^3$, $C_{PI} = 15$ wt%) at 30 °C and six-arm star PI ($M_{arm} = 179 \times 10^3$, $C_{PI} = 20$ wt%) at 25 °C. For comparison, the ε'' data at equilibrium ($\dot{\gamma} = 0$) are also shown. Redrawn, with permission, from 2002 *Macromolecules* **35** 8802–18. Copyright 2002 Am. Chem. Soc.

in terms of the chain conformation ($\tilde{\boldsymbol{u}}$) as

$$\Delta\varepsilon(\dot{\gamma}) = K_\varepsilon \nu a^2 \sum_{all\,n}^{N_{chain}} \sum_{all\,m}^{N_{chain}} \langle \tilde{u}_y(n,0)\tilde{u}_y(m,0)\rangle \qquad (K_\varepsilon = K'_\varepsilon \mu_0^2). \tag{5}$$

Here, ν represents the chain number density, and N_{chain} is the number of entanglement segments per chain. For the nth and mth segments belonging to different chains, the opposite configurations $\tilde{\boldsymbol{u}}(n,0)\tilde{\boldsymbol{u}}(m,0)$ and $-\tilde{\boldsymbol{u}}(n,0)\tilde{\boldsymbol{u}}(m,0)$ are realized with the same probability and the average $\langle \tilde{\boldsymbol{u}}(n,0)\tilde{\boldsymbol{u}}(m,0)\rangle$ vanishes. Considering this feature, we have limited the summation in equation (5) to the segments in the same chain.

In equation (5), the $\langle \tilde{\boldsymbol{u}}_y(n,0)\tilde{\boldsymbol{u}}_y(m,0)\rangle$ term with $n \neq m$ represents the isochronal, orientational cross-correlation of two entanglement segments characterizing the non-Gaussian conformation under flow. Since this cross-correlation would not extend over the whole backbone of the chain (unless the chain is fully stretched), we may introduce a cut-off number β and consider that the cross-correlation only survives in a sequence of the successive β entanglement segments [10]. Then, equation (5) is rewritten as

$$\Delta\varepsilon(\dot{\gamma}) = K_\varepsilon \nu N_{chain} a^2 \{\langle \tilde{u}_y^2\rangle + (\beta - 1)\langle \tilde{u}_y \tilde{u}'_y\rangle\}. \tag{6}$$

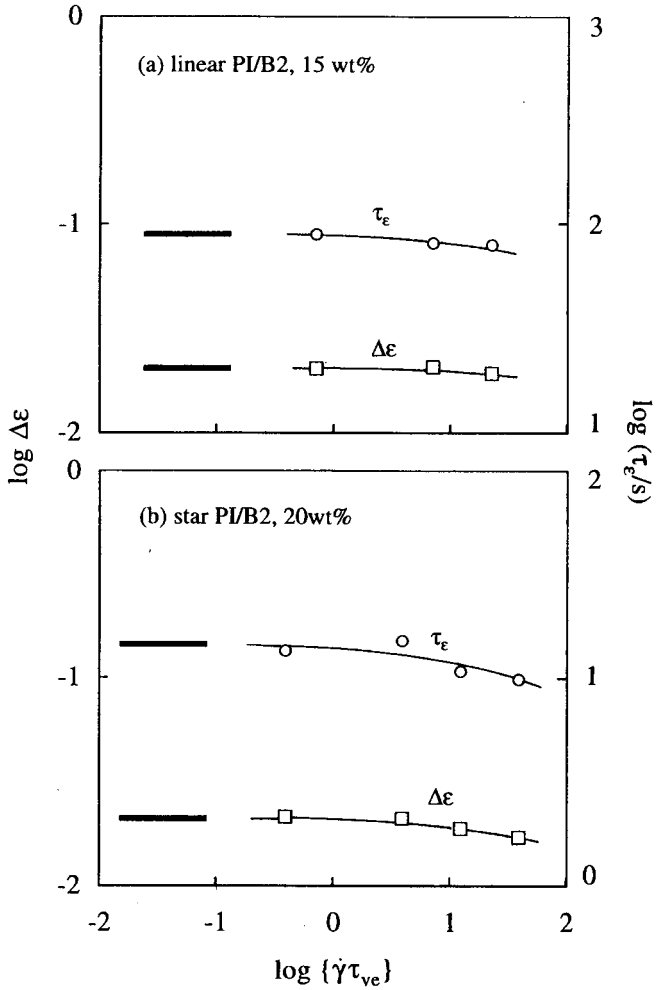

Figure 7. Plots of the dielectric intensity $\Delta\varepsilon$ and terminal dielectric relaxation time τ_ε of entangled linear PI ($M_w = 1190 \times 10^3$, $C_{PI} = 15$ wt%) at 30 °C and six-arm star PI ($M_{arm} = 179 \times 10^3$, $C_{PI} = 20$ wt%) at 25 °C against the normalized shear rate $\dot{\gamma}\tau_{ve}$. Redrawn, with permission, from 2002 *Macromolecules* **35** 8802–18. Copyright 2002 Am. Chem. Soc.

Here, $\langle\tilde{u}_y^2\rangle$ is the average taken for all entanglement segments, and $\langle\tilde{u}_y\tilde{u}_y'\rangle$ is the cross-correlation averaged over the sequence of β segments.

At equilibrium ($\dot{\gamma} = 0$), the chain has the Gaussian conformation and the cross-correlation vanishes. For this case, we find $\langle\tilde{u}_y(n,0)\tilde{u}_y(m,0)\rangle = \delta_{nm}/3$ and $\Delta\varepsilon(0) = K_\varepsilon \nu N_{chain} a^2/3$ [10]. Thus, the ratio of $\Delta\varepsilon(\dot{\gamma})$ under the flow to $\Delta\varepsilon(0)$ is expressed as

$$\frac{\Delta\varepsilon(\dot{\gamma})}{\Delta\varepsilon(0)} = 3\langle\tilde{u}_y^2\rangle + 3(\beta - 1)\langle\tilde{u}_y\tilde{u}_y'\rangle. \tag{7}$$

The average $3\langle\tilde{u}_y^2\rangle$ appearing in equation (7) can be determined viscoelastically. For the unstretched (but oriented) chains under the shear flow, the first and second normal stress coefficients are related to the components of $\tilde{u}$ as [1, 2, 10]

$$\Psi_1 = \frac{3G_N}{\dot{\gamma}^2}\{\langle\tilde{u}_x^2\rangle - \langle\tilde{u}_y^2\rangle\}, \qquad \Psi_2 = \frac{3G_N}{\dot{\gamma}^2}\{\langle\tilde{u}_x^2\rangle + 2\langle\tilde{u}_y^2\rangle - 1\} \tag{8}$$

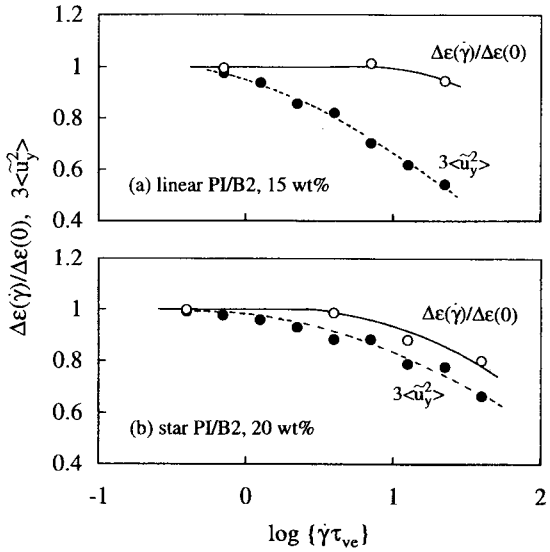

Figure 8. Comparison of the dielectrically determined $\Delta\varepsilon(\dot\gamma)/\Delta\varepsilon(0)$ ratio and the viscoelastically evaluated $3\langle\tilde u_y^2\rangle$ of entangled linear PI ($M_w = 1190 \times 10^3$, $C_{PI} = 15$ wt%) at 30 °C and six-arm star PI ($M_{arm} = 179 \times 10^3$, $C_{PI} = 20$ wt%) at 25 °C. A difference between $\Delta\varepsilon(\dot\gamma)/\Delta\varepsilon(0)$ and $3\langle\tilde u_y^2\rangle$ indicates the flow-induced orientational cross-correlation of successive entanglement segments. Redrawn, with permission, from 2002 *Macromolecules* **35** 8802–18. Copyright 2002 Am. Chem. Soc.

where $\tilde u_x$ is the component in the shear direction. In the thinning regime similar to that examined in figure 5, literature data indicate that Ψ_2 is close to $-0.1\Psi_1$ [24–26]. Thus, $3\langle\tilde u_y^2\rangle$ was evaluated from the Ψ_1 data (figure 5) as $3\langle\tilde u_y^2\rangle = 1 - \{1.1\dot\gamma^2\Psi_1/3G_N\}$.

For the linear and star PI chains, figure 8 shows plots of this $3\langle\tilde u_y^2\rangle$ and the $\Delta\varepsilon(\dot\gamma)/\Delta\varepsilon(0)$ ratio (evaluated from the $\Delta\varepsilon$ data; figure 7) against the normalized shear rate $\dot\gamma\tau_{ve}$. The $3\langle\tilde u_y^2\rangle$ significantly decreases from unity (equilibrium value) with increasing $\dot\gamma\tau_{ve} > 1$, confirming that the entanglement segments are highly shear oriented (tilted) toward the shear direction. (This orientation was also noted from an average $\langle\tilde u_x\tilde u_y\rangle$ evaluated from the η data [10].) More importantly, a difference between $\Delta\varepsilon(\dot\gamma)/\Delta\varepsilon(0)$ and $3\langle\tilde u_y^2\rangle$, representing the cross-correlation $3(\beta - 1)\langle\tilde u_y\tilde u_y'\rangle$ shown in equation (7), increases with $\dot\gamma\tau_{ve}$. Thus, the shear-orientation of the entanglement segments resulting in the thinning is associated with the growth of their cross-correlation. This conclusion was obtained at all C_{PI} examined [10].

The isochronal, orientational cross-correlation never emerges if respective entanglement segments behave as *independent* stress-sustaining units. Thus, the above results unequivocally indicate that some successive segments are *mutually equilibrated* and orientationally correlated to behave together as an enlarged stress-sustaining unit under the flow in the thinning regime.

4.3. Current molecular picture and problems

For entangled chains, the tube model considers that the motion of a given chain (probe) is constrained in a tubelike region having a non-crossable wall. In the current model, this tube can move with time as a result of the motion of the surrounding, tube-forming chains [1, 2]. Because of this tube motion, an *effective* tube constraining the probe motion dilates with time [27, 28], and the probe segments included in an enlarged tube segment are mutually equilibrated. Under

the shear flow at $\tau_{ve}^{-1} < \dot{\gamma} < \tau_R^{-1}$, the tube motion resulting in this dynamic tube dilation (DTD) is activated dominantly by the flow-induced motion of the tube-forming chains: these chains, transiently stretched by the flow, shrink to recover their equilibrium contour length, and this shrinkage allows the tube to move. This mechanism of the flow-induced tube motion is referred to as the convective constraint release (CCR) [29–31].

The rheo-dielectrically detected mutual equilibration of the entanglement segments under the shear flow is attributable to this CCR-induced DTD process. On the basis of this assignment, the average segment number β for the flow-induced cross-correlation was estimated from the $\Delta\varepsilon(\dot{\gamma})/\Delta\varepsilon(0)$ and $3\langle\tilde{u}_y^2\rangle$ data: $\beta \cong 1.8$ and 1.2 for the linear and star PI chains at the largest $\dot{\gamma}$ examined in the rheo-dielectric test, and the difference between the β values of the linear and star chains can be related to a difference in their constraint release processes at equilibrium [10]. Thus, within the CCR–DTD molecular picture, the observed difference between $\Delta\varepsilon(\dot{\gamma})/\Delta\varepsilon(0)$ and $3\langle\tilde{u}_y^2\rangle$ is attributable to a physically plausible magnitude of cross-correlation (with β not much larger than unity). This result suggests a fundamental validity of this picture.

Now, we turn our attention to the flow-induced decrease of the dielectric relaxation time τ_ε (figure 7). For the star PI chain, τ_ε scales with M_e and M_{arm} as $\exp(\nu' M_{arm}/M_e)$ with $\nu' \cong 0.6$ [1, 2]. The mutual equilibration explained above corresponds to an increase of an effective M_e by a factor of β, and τ_ε is expected to decrease by a factor of $\exp(\{\beta^{-1} - 1\}\nu' M_{arm}/M_e)$ on this equilibration. This expectation was quantitatively confirmed from the τ_ε data [10], lending support for the CCR–DTD picture.

However, problems still remain for the linear PI chain having $\tau_\varepsilon \propto M^{3.5}/M_e^{1.5}$. The above β value ($\cong$1.8) gave a decrease of τ_ε much more significant than the observed decrease [10]. In addition, the current CCR model formulated for the viscoelastic relaxation [29–31] can be extended to the dielectric relaxation, and the simplest extension suggests a strong decrease of τ_ε under flow (by a factor $\propto \dot{\gamma}^{-1}$) in contradiction to the observation [10]. A further study is necessary for these problems.

5. Concluding remarks

In this article, we have demonstrated that the rheo-dielectric method enables us to reveal novel non-equilibrium features of the type-B OS molecules and type-A PI chains: the extraordinary strong shear thinning of OS is related to the flow-induced acceleration of the segmental motion that possibly results from a reduction of the cooperativity of the segmental motion. For the entangled PI chains, the moderate decreases of the dielectric intensity $\Delta\varepsilon$ and relaxation time τ_ε observed under the shear flow are related to a flow-induced orientational cross-correlation of the entanglement segments. This cross-correlation is consistent with the CCR–DTD molecular picture in the tube model for entangled chains, although the current CCR model does not seem to accurately describe the shear rate dependence of τ_ε of the linear chain.

The usefulness of the rheo-dielectric method is not limited to uniform systems of oligomeric and polymeric molecules. In fact, this method has been successfully applied to various non-uniform (multi-phase) systems: for example, a heterogeneity of the flow field in microphase-separated ABA-type triblock copolymer systems [5] and a relationship between the shear-orientation and size of smectic liquid crystalline domains [8] were rheo-dielectrically investigated. Furthermore, a related method measuring the direct current conductance under flow was successfully applied to a suspension of aggregating carbon-black particles to detect the flow-induced disruption of the aggregates [32].

Thus, the rheo-dielectric method serves as a powerful tool for investigation of non-equilibrium phenomena under flow. This method deserves further attention.

Acknowledgments

This work was partly supported by the Ministry of Education, Culture, Sports, Science, and Technology, Japan (grant no 13450391). YM acknowledges, with thanks, financial support from a JSPS Research Fellowship for Young Scientists.

References

[1] Doi M and Edwards S F 1986 *The Theory of Polymer Dynamics* (Oxford: Clarendon)
[2] Watanabe H 1999 *Prog. Polym. Sci.* **24** 1253
[3] Janeschitz-Kriegl H 1983 *Polymer Melt Rheology and Flow Birefringence* (Berlin: Springer)
[4] Fuller G G 1995 *Optical Rheometry* (New York: Oxford University Press)
[5] Sato T, Watanabe H and Osaki K 1996 *Macromolecules* **29** 6231
[6] Matsumiya Y, Watanabe H, Inoue T, Osaki K and Yao M L 1998 *Macromolecules* **31** 7973
[7] Watanabe H, Sato T, Hirose M, Osaki K and Yao M L 1998 *Rheol. Acta* **37** 519
[8] Watanabe H, Sato T, Hirose M, Osaki K and Yao M L 1999 *Rheol. Acta* **38** 100
[9] Watanabe H, Sato T, Matsumiya Y, Inoue T and Osaki K 1999 *J. Soc. Rheol. Japan* **27** 121
[10] Watanabe H, Ishida S and Matsumiya Y 2002 *Macromolecules* **35** 8802
[11] Riande E and Saiz E 1992 *Dipole Moments and Birefringence of Polymers* (Englewood Cliffs, NJ: Prentice-Hall)
[12] Cole R H 1965 *J. Chem. Phys.* **42** 637
[13] Inoue T, Okamoto H and Osaki K 1991 *Macromolecules* **24** 5670
[14] Inoue T, Ryu D S and Osaki K 1998 *Macromolecules* **31** 6977
[15] Ferry J D 1980 *Viscoelastic Properties of Polymers* (New York: Wiley)
[16] Stockmayer W H 1967 *Pure Appl. Chem.* **15** 539
[17] Imanishi Y, Adachi K and Kotaka T 1988 *J. Chem. Phys.* **89** 7585
[18] Watanabe H 2001 *Macromol. Rapid Commun.* **22** 127
[19] Graessley W W 1974 *Adv. Polym. Sci.* **16** 1
[20] Yamamoto R and Onuki A 1997 *Europhys. Lett.* **40** 61
[21] Kanaya T, Patkowski A, Fischer E W, Seils J, Gläser H and Kaji K 1995 *Macromolecules* **28** 7831
[22] Matsuoka S 1992 *Relaxation Phenomena in Polymers* (New York: Hanser)
[23] Watanabe H, Matsumiya Y and Inoue T 2002 *Macromolecules* **35** 2339
[24] Osaki K, Kimura S and Kurata M 1981 *J. Polym. Sci. Polym. Phys. Edn* **19** 517
[25] Magda J, Lee C S, Muller S J and Larson R G 1993 *Macromolecules* **26** 1696
[26] Broan E F, Burghardt W R, Kahvand H and Venerus D C 1995 *Rheol. Acta* **34** 221
[27] Marrucci G 1985 *J. Polym. Sci. Polym. Phys. Edn* **23** 159
[28] Ball R C and McLeish T C B 1989 *Macromolecules* **22** 1911
[29] Ianniruberto G and Marrucci G 1996 *J. Non-Newton. Fluid Mech.* **65** 241
[30] Mead D W, Larson R G and Doi M 1998 *Macromolecules* **31** 7895
[31] Milner S T, McLeish T C B and Likhtman A E 2001 *J. Rheol.* **45** 539
[32] Watanabe H, Matsumiya Y, Kakiuchi M and Aoki Y 2001 *J. Soc. Rheol. Japan* **29** 77